

# Enhanced Spectral Shaping in Steady-State Free Precession Imaging

Tolga Çukur,<sup>1,\*</sup> Neal K. Bangerter,<sup>2</sup> and Dwight G. Nishimura<sup>1</sup>

**Balanced steady-state free precession (SSFP) is hindered by the inherent off-resonance sensitivity and unwanted bright fat signal. Multiple-acquisition SSFP combination methods, where multiple datasets with different fixed RF phase increments are acquired, have been used for shaping the SSFP spectrum to solve both problems. We present a new combination method (weighted-combination SSFP or WC-SSFP) that preserves SSFP contrast and enables banding-reduction and fat-water separation. Methods addressing the banding artifact have focused on either getting robust banding-reduction (complex-sum SSFP) or improved SNR efficiency (sum-of-squares SSFP). The proposed method achieves both robust banding-reduction and an SNR efficiency close to that of the sum-of-squares method. A drawback of fat suppression methods that create a broad stop-band around the fat resonance is the wedge shape of the stop-band leading to imperfect suppression. WC-SSFP improves the suppression of the stop-band without affecting the pass-band performance, and prevents fat signal from obscuring the tissues of interest in the presence of considerable resonant frequency variations. The method further facilitates the use of SSFP imaging by providing a control parameter to adjust the level of banding-reduction or fat suppression to application-specific needs. Magn Reson Med 58:1216–1223, 2007. © 2007 Wiley-Liss, Inc.**

**Key words:** SSFP; phase cycling; banding artifact; SNR efficiency; fat-water separation

## INTRODUCTION

Balanced steady-state free precession (SSFP) sequences (1–3) have gained popularity in magnetic resonance imaging (MRI) as they can yield high signal-to-noise ratios (SNR) within very short scan times. However, there are several problems limiting the applicability of SSFP imaging. The balanced SSFP signal is a function of the local resonant frequency, leading to characteristic signal nulls/voids (known as banding artifacts) in regions of large resonant frequency variation. Furthermore, the bright lipid signal is often undesired.

At higher field strengths or with longer repetition times (TR), the banding artifacts become more pronounced. It is therefore necessary to limit the off-resonance frequency

variation to approximately  $2/(3 * TR)$  to avoid any banding artifacts (4). However, it is not always possible to limit the repetition time as specific absorption rate (SAR) considerations and resolution requirements may place constraints on the minimum TR. A longer minimum TR due to increased power deposition and resonant frequency variations at higher fields can potentially lead to severe banding artifacts.

A common strategy to reduce these artifacts has been to acquire a plurality of SSFP images, where the radio-frequency (RF) pulse phase increment between successive TRs is changed with each acquisition (5,6) to shift the spectral response of the signal. Several methods for combining these multiple acquisitions have been proposed, including maximum-intensity (MI) (7), complex-sum (CS) (8), magnitude-sum and sum-of-squares (SOS) (9) combinations, and the nonlinear averaging reconstruction method (10). The complex-sum method aims to reduce banding artifacts but is far from optimal in terms of SNR efficiency. On the other hand, the magnitude-sum and SOS methods yield higher SNR efficiencies but provide less robust suppression of banding artifacts.

It is necessary to suppress the fat signal in applications where the tissue of interest has comparable or smaller signal than fat, including coronary artery imaging (11), cartilage imaging (12) and flow-independent angiography (13). There are various methods for suppression; one common way of reducing the fat signal in SSFP is to shape the periodic frequency response such that a broad range of frequencies around the resonant frequency of lipid are selectively masked out. Recent examples of this group of methods include fluctuating equilibrium magnetic resonance (FEMR) (14), linear combination SSFP (LC-SSFP) (8), binomial excitation patterns (15), periodic flip angle variations (16,17), and fat suppressing alternating TR (FS-ATR) SSFP (18).

A drawback of these methods is the wedge shape of the stop-bands. The relatively broad stop-bands fail to yield suppression over certain ranges of frequencies, leading to a residual fat signal comparable to the water signal. Consequently, moderate to large resonant frequency variations will compromise the robustness of fat suppression.

In this work, we present a new method (weighted-combination SSFP or WC-SSFP) for combining a plurality of SSFP images with different RF phase increments for improved shaping of the SSFP profile and demonstrate its applicability to banding artifact reduction and fat-water separation. Our method approaches the SNR efficiency of the SOS method, while reducing the banding artifacts as effectively as the CS method by weighting each SSFP dataset by a power (greater than 1) of its magnitude. The exact value of the power is a control parameter which adjusts the trade-off between banding artifact reduction

<sup>1</sup>Magnetic Resonance Systems Research Laboratory, Department of Electrical Engineering, Stanford University, Stanford, California

<sup>2</sup>Department of Radiology, Stanford University, Stanford, California

Contract grant sponsor: National Institutes of Health (NIH); Contract grant numbers: R01 HL039297, R01 HL 075803,

Contract grant sponsors: GE Healthcare, Rambus Corporation Stanford Graduate Fellowship

\*Correspondence to: Tolga Çukur, Packard Electrical Engineering, Room 210, 350 Serra Mall, Stanford, CA 94305-9510. E-mail: cukur@stanford.edu

Received 4 April 2007; revised 2 August 2007; accepted 19 August 2007.

DOI 10.1002/mrm.21413

Published online 26 October 2007 in Wiley InterScience (www.interscience.wiley.com).

and SNR efficiency, giving greater flexibility for image optimization. The favorable SNR efficiency properties and robust banding artifact reduction coupled with this flexibility to tune for specific applications will allow higher field SSFP imaging, higher resolution or reduced SAR imaging over a greater range of TRs and with reduced banding artifact.

We further propose a new SSFP combination method for improved fat suppression. The LC-SSFP method produces a stop-band centered at the fat resonance by combining two phase-cycled SSFP acquisitions. The two combined magnetization profiles are out-of-phase in the vicinity of the fat resonance. Consequently, the two profiles are subtracted from each other. Since the magnitudes of the subtracted profiles are not the same for all frequencies, there is residual stop-band signal in the final image. The performance of the LC-SSFP method degrades at higher flip angles and when the tissue sample has a relatively low T1/T2 ratio. Weighting SSFP datasets by a negative power (between  $-1$  and  $0$ ) of their magnitudes and combining them as in LC-SSFP achieves a drastic improvement in suppression robustness without affecting the pass-band. The range of flip angles and T1/T2 ratios for which LC-SSFP works robustly are expanded. The level of stop-band suppression can be adjusted through the power control parameter to meet application-specific needs. 2D and 3D fat- or water-suppressed SSFP imaging in the presence of large off-resonant frequency variations and at higher resolutions can be successfully accomplished with the proposed method.

## METHODS

### Banding Artifact Reduction

The signal null in the SSFP spectrum leads to regions of signal loss in the resultant images. The challenge in banding artifact reduction is to create as flat a signal profile as possible. Multiple-acquisition methods that target removal of banding artifacts differ in the way they combine the SSFP datasets (9). The CS method yields robust banding artifact reduction; however, phase incoherences across the datasets lead to signal loss and reduced SNR efficiency. On the other hand, the SOS technique weights each dataset by its own magnitude for optimal SNR properties. Nonetheless, its banding removal performance does not match that of the CS method.

The proposed method is a hybrid of these techniques that tries to preserve the favorable properties of each. Assuming there are  $N$  separate SSFP images, the  $n$ th image being  $X_n$ , the resulting image  $Y$  can be expressed as,

$$Y = \left| \sum_{n=1}^N |X_n|^p X_n \right|^{\left(\frac{1}{1+p}\right)}, \quad [1]$$

where  $p$  is the control parameter mentioned previously. The final raising to the  $\left(\frac{1}{1+p}\right)$ th power is necessary to restore the initial image contrast, which is modified by the magnitude-to-a-power weighting of the individual datasets. The proposed method sums complex SSFP signals weighted by their magnitudes when  $p = 1$ , as opposed to

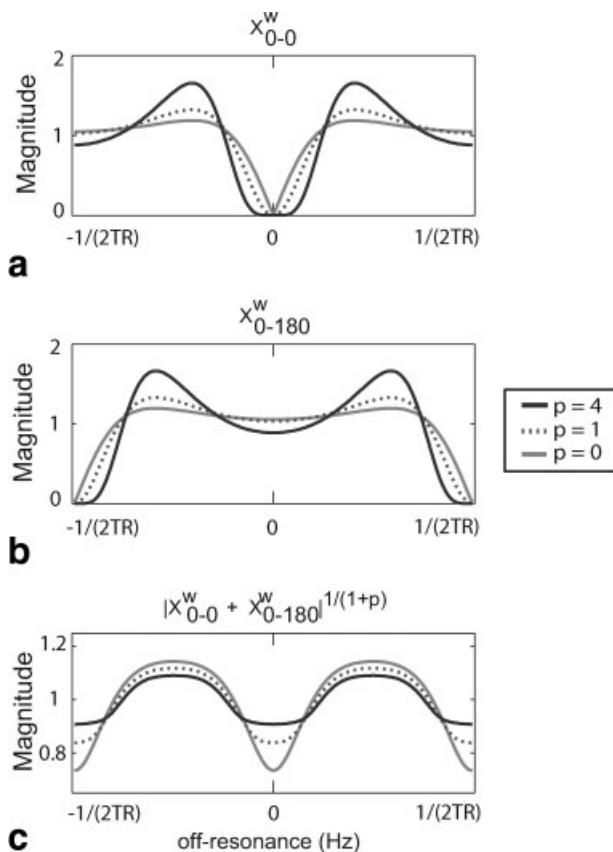


FIG. 1. Magnitude spectra of SSFP datasets after magnitude-to-a-power weighting ( $X^w = |X|^p X$ ), with (a) 0–0 ( $\Delta\phi = 0$ ) and (b) 0–180 ( $\Delta\phi = \pi$ ) phase cycling. The spectrum of the combination is shown in c for a range of  $p$ -values. The combined profile becomes flatter as  $p$  is increased. All the displayed magnitude profiles have been normalized with respect to their mean. Note that the vertical display scale in c is different from the scale in a and b.

the square of the magnitudes in SOS combination. When  $p = 0$ , the method is equivalent to CS combination. For very large  $p$ , the weighted complex-sum method approaches the MI method.

The effects of magnitude-to-a-power weighting on the SSFP profile and the resulting combination are displayed in Fig. 1. A flip angle of  $\alpha = 30^\circ$  and a T1/T2 = 1,000/200 ms were assumed. When the individual datasets are weighted by a positive power of their magnitude, the high signal points in the spectrum are weighted more heavily than the low signal points. Improved banding artifact reduction is achieved because of the diminishing effect of the SSFP nulls on the resulting combination as  $p$  is increased. It should be noted that the adverse effect of the initial weighting on the uniformity of the SSFP profile is reverted by the power  $\left(\frac{1}{1+p}\right)$  operation at the end.

The formalism outlined by Bangerter et al. (9) was used for a quantitative comparison between their proposed method (SOS) and the then-existing methods (MI,CS). In this formalism, each of the multiple SSFP acquisitions is modeled as a bivariate Gaussian random variable and the average SNR of the resulting image is computed over a

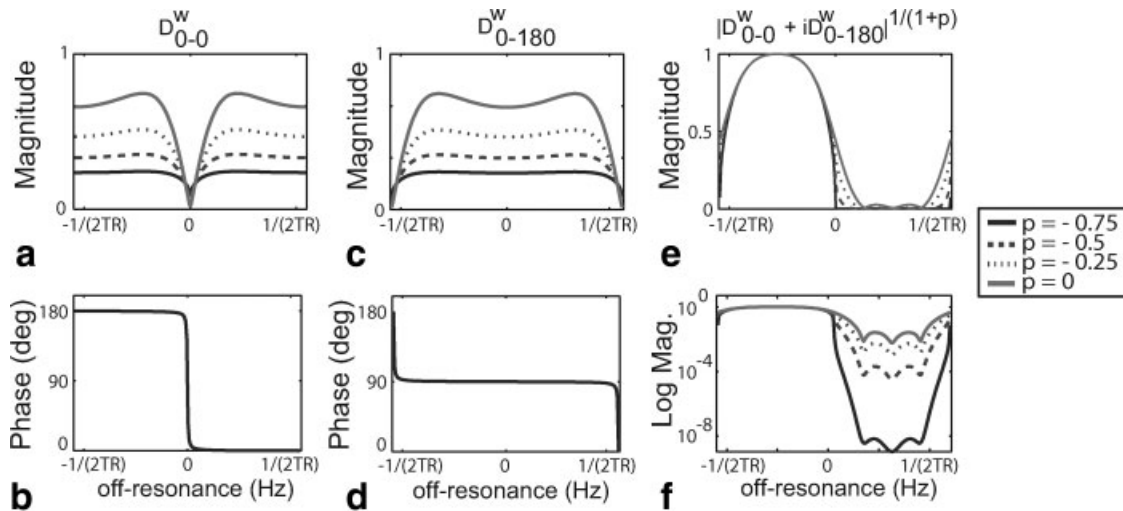


FIG. 2. Magnitude and phase spectra of SSFP datasets after magnitude-to-a-power weighting ( $D^w = |D|^p D$ ), with (a–b) 0–0 ( $\Delta\phi = 0$ ) and (c–d) 0–180 ( $\Delta\phi = \pi$ ) phase cycling. The spectra of the combined datasets corresponding to the water image are shown in (e) linear and (f) logarithmic scales for a range of  $p$  values. The improvement in the stop-band suppression as  $p$  is decreased toward  $-1$  can clearly be seen in f.

period of the resonant-frequency variation. A good measure for the banding artifact reduction of any combination method is the percent ripple of a period of the spectrum of the resulting image.

Simulated SSFP phantom images with two different phase-cycling schemes, namely 0–0 and 0–180, were generated to verify the theory. The phantom consisted of three strips of tissues with the following relaxation parameters:  $T1/T2 = 270/85$  ms for fat,  $870/47$  ms for muscle and  $1,000/200$  ms for arterial blood. An echo time (TE) of 5 ms, a TR of 10 ms and  $\alpha = 30^\circ$  were assumed. The off-resonance frequency was linearly varied in the horizontal direction. An individual SSFP image SNR of 15 at the center of the pass-band for fat was achieved by adding bivariate Gaussian noise to the data. The data were combined with the CS, SOS, and WC methods.

The CS, SOS, WC ( $p = 1$ ), and nonlinear averaging reconstruction (only for  $N = 4$ ) methods were also compared in terms of percent ripple and SNR efficiency for a range of simulation parameters:  $\alpha = 30^\circ$  and  $60^\circ$ ,  $TR/TE = 10/5$  ms,  $T1 = 300$ – $2,000$  ms and  $T2 = 50$ – $220$  ms. Simulations were performed for both  $N = 2$  and  $N = 4$ , and an SNR of 15 was assumed at the center of the pass-band for a single SSFP acquisition.

The performance of the method was also tested with doped  $MnCl_2$  phantoms. 3D balanced SSFP images of three phantoms were acquired on a 1.5 T GE Signa Excite scanner with CV/i gradients with the following parameters:  $\alpha = 30^\circ$ , 16 cm FOV,  $0.5 \times 0.5 \times 2$  mm<sup>3</sup> resolution,  $TR/TE = 20/10$  ms, 30 kHz bandwidth and four different phase-cycling schemes ( $\Delta\phi = 0, \pi/2, \pi, 3\pi/2$ ). The relaxation parameters for the phantoms were  $T1/T2 = 1,300/900, 800/375, 250/50$  ms respectively. The CS, SOS, nonlinear averaging reconstruction and WC ( $p = 1$ ) methods were used to combine the data.

In vivo 3D balanced SSFP images of a volunteer's brain were acquired on a 1.5 T GE Signa Excite scanner with the

following parameters:  $TR/TE = 15/7.2$  ms,  $0.67 \times 1.3 \times 4$  mm<sup>3</sup> resolution (zero-padded to  $0.67 \times 0.67 \times 4$  mm<sup>3</sup>),  $\alpha = 30^\circ$ ,  $384 \times 192 \times 16$  encoding, 31.25 kHz readout bandwidth, two different phase-cycling schemes ( $\Delta\phi = 0, \pi$ ) and a total scan time of 1:32. The acquisitions were combined with the CS, SOS, and WC ( $p = 1$ ) methods.

#### Fat-Water Separation

The off-resonance dependence of the phase of the SSFP signal makes it feasible to create stop- and pass-bands through the linear combination of two phase-cycled images with different RF phase increments (8). By proper selection of TR (2.3 ms at 1.5 T), the separation between the centers of these two bands can be adjusted to match the fat/water frequency separation,  $\sim 217$  Hz at 1.5 T. Therefore, we can selectively reconstruct fat and water images by swapping the stop- and pass-band locations.

In LC-SSFP (equivalently WC-SSFP for  $p = 0$ ), two SSFP datasets  $D_{0-0}$  and  $D_{0-180}$ , with RF phase increments  $\Delta\phi = 0^\circ$  and  $180^\circ$  respectively, are acquired. The phase difference between the data sets is  $\pi/2$  radians for one-half of the spectral period and  $-\pi/2$  radians for the other half as displayed in Fig. 2a–d. A flip angle of  $\alpha = 30^\circ$  and a  $T1/T2 = 1,000/200$  ms were assumed. Therefore, a summation of  $D_{0-0}$  with the  $\pi/2$  radians phase-shifted version of  $D_{0-180}$  creates stop- and pass-bands. The transverse magnetization values in the two

Table 1  
The Percent Ripple and SNR of Three Tissues in the Phantom Images for the WC ( $p = 1, 4$ ), CS and SOS Combination Methods

Tissue	$p = 1$	$p = 4$	CS	SOS
Fat	34%, 20.3	30%, 18.4	31%, 17.4	44%, 22.7
Muscle	16%, 8.6	10%, 8.1	24%, 7.2	28%, 9.2
Blood	31%, 16.4	22%, 15.2	40%, 13.5	44%, 18.6

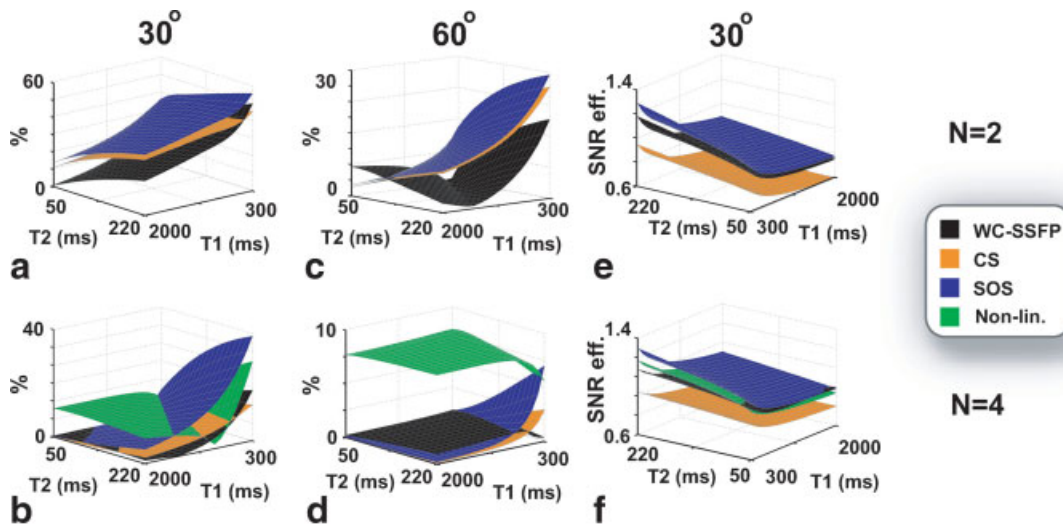


FIG. 3. The percent ripple and SNR efficiency of the CS, SOS, WC ( $p = 1$ ) and nonlinear averaging reconstruction methods (only for  $N = 4$ ). (a,c,e)  $N = 2$  and (b,d,f)  $N = 4$ , (a,b,e,f)  $\alpha = 30^\circ$  and (c,d)  $\alpha = 60^\circ$  respectively. The SNR efficiency results for  $\alpha = 60^\circ$  are not displayed as the relative performance of the methods is almost equivalent to the case for  $\alpha = 30^\circ$ . For a wide range of  $T_1$ ,  $T_2$  values the percent ripple of the WC-SSFP technique is smaller than that for the other methods, while the SNR efficiency of the WC method is very close to the efficiency of the SNR-optimal SOS method. The improvement in banding artifact reduction over the CS and SOS methods is more pronounced with a smaller number of total acquisitions ( $N = 2$ ).

different spectra subtracted from each other are not equal because of the shape of the SSFP spectrum and the presence of signal nulls. Hence, the stop-band will display deviations from a perfect null for certain ranges of frequencies. For this reason, the reduced flatness of the SSFP spectrum with higher flip angles and lower  $T_1/T_2$  ratios decreases the robustness of the fat-water separation in LC-SSFP.

The range of magnetization amplitudes observed with off-resonance frequency variation are reduced if the SSFP dataset is weighted by its magnitude raised to a negative power  $p$  between  $-1$  and  $0$  as shown in Fig. 2a,c. If the difference in the magnitude of magnetization between the two datasets is decreased, then the stop-band will get closer to a perfect null. The magnitude of each signal can be raised to a power and used as a weighting factor before linearly combining the two. The resulting water image  $Y_w$  and fat image  $Y_f$  can be expressed as

$$Y_w = ||D_{0-0}|^p D_{0-0} + i|D_{0-180}|^p D_{0-180}|^{\left(\frac{1}{1+p}\right)}, \quad [2]$$

$$Y_f = ||D_{0-0}|^p D_{0-0} - i|D_{0-180}|^p D_{0-180}|^{\left(\frac{1}{1+p}\right)}, \quad [3]$$

where  $p$  is the parameter adjusting the level of suppression and is to be varied in the range  $(-1, 0]$ . The  $\left(\frac{1}{1+p}\right)$ th power of the combined image restores the original contrast that would be captured with the LC-SSFP method. The method is exactly equivalent to LC-SSFP for  $p = 0$ . The stop-band suppression improves with decreasing values of the parameter as displayed in Fig. 2e,f. It is important to note that  $p = -1$  is not feasible as it removes all tissue contrast irreversibly.

The effective stop-band suppression of the WC-SSFP method was demonstrated on a water phantom ( $T_1/T_2 =$

250/50 ms). A linear shim gradient in the readout direction was employed to simulate the off-resonance spectrum and create alternating pass- and stop-bands along the phantom. The images were acquired with flip angles of  $30^\circ$  and  $60^\circ$ .

The improvement in stop-band suppression can be quantified by computing the ratio of the average water signal within a pass-band to the average fat signal within a stop-band. The flip angle and  $p$  dependency of the ratio was simulated for the following set of parameters:  $T_1/T_2 = 1,000/100$  ms for the water tissue,  $T_1/T_2 = 270/85$  ms for the fat tissue,  $TR/TE = 2.3/1.15$  ms. The effective width of the stop-band at  $TR = 2.3$  ms is  $\sim 160$  Hz. Therefore the pass-band was chosen to be the interval  $[-80$  Hz,  $80$  Hz], whereas the stop-band was within  $[-300$  Hz,  $-140$  Hz].

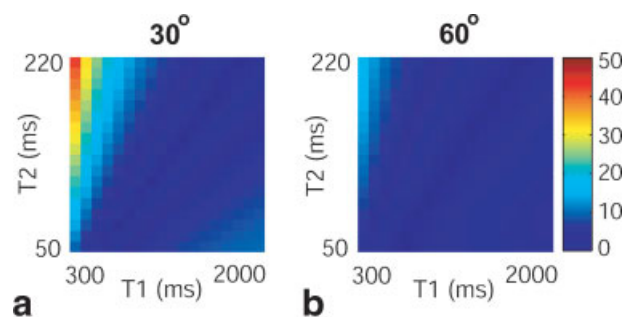


FIG. 4. The percentage change (from the center of the pass-band SSFP signal to the average pass-band WC-SSFP signal) was computed for a range of  $T_1$  and  $T_2$  values assuming (a)  $\alpha = 30^\circ$  and (b)  $\alpha = 60^\circ$ . The following simulation parameters were used:  $TR/TE = 10/5$  ms,  $N = 2$  and  $p = 1$  for WC-SSFP. The WC-SSFP contrast is similar to the basic SSFP contrast.

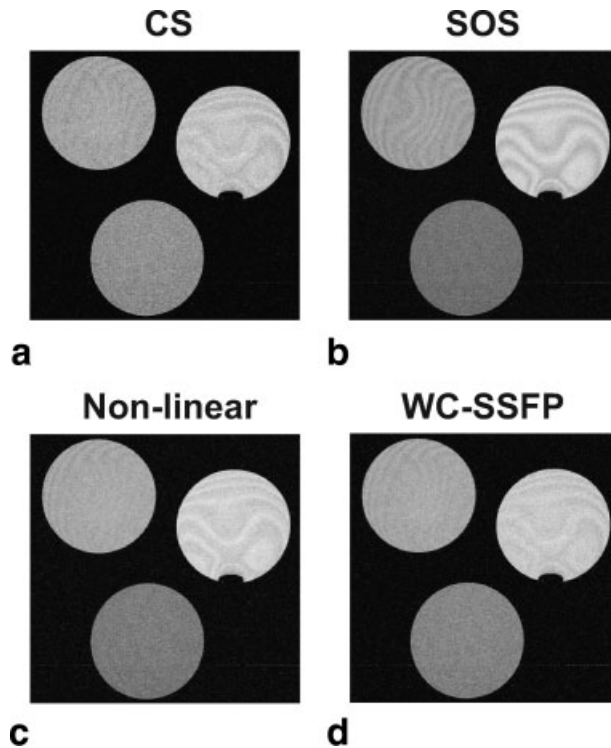


FIG. 5. 3DFT – SSFP images of three phantoms with  $T_1/T_2 = 1,300/900$  (upper-right),  $800/375$  (upper-left),  $250/50$  (bottom) ms, were acquired with  $\alpha = 30^\circ$ , 16 cm FOV,  $0.5 \times 0.5 \times 2$  mm<sup>3</sup> resolution, TR/TE = 20/10 ms, 30 kHz bandwidth and 4 different phase-cycling schemes ( $\Delta\phi = 0, \pi/2, \pi, 3\pi/2$ ). Combination images are displayed for (a) CS, (b) SOS, (c) nonlinear averaging reconstruction and (d) WC ( $p = 1$ ) methods. The WC-SSFP method delivers the most robust banding artifact reduction with near-optimal SNR efficiency.

The improved stop-band suppression of the WC-SSFP method was also demonstrated in vivo. Two 3D SSFP acquisitions on a 1.5 T GE Signa Excite scanner with CV/i gradients were performed on a volunteer's knee with the following parameters: TR = 2.7 ms, 1 mm isotropic resolution,  $\alpha = 30^\circ$ ,  $192 \times 128 \times 128$  encoding, 250 kHz bandwidth and a total scan time of 1:18.

## RESULTS

### Banding Artifact Reduction

Individual SSFP phantom images were simulated and CS, SOS, and weighted combination (WC, with two different values of the parameter  $p$ ) methods were used to combine them. The WC-SSFP method is more successful at reducing banding artifacts than both the CS and the SOS methods, while achieving an SNR close to that of the SOS method. The optimal SNR is achieved when  $p = 1$ , similar to SOS combination. The artifact reduction is improved with an accompanying decrease in average SNR by increasing  $p$  to 4 as expected. The percent ripple and average SNR measurements of each tissue across the spectrum with different methods are listed in Table 1.

The results for the percent ripple and SNR efficiency simulations are shown in Fig. 3. The banding artifact reduction performance of the WC method is superior to that of

the other methods for a range of  $T_1$  and  $T_2$  values commonly found in vivo, without a substantial compromise in SNR efficiency over the optimal-SNR SOS combination.

The contrast of SSFP and WC-SSFP images can be compared by computing the percentage change from the center of the pass-band signal of SSFP to the average signal of the WC-SSFP spectrum. The percentage change is displayed in Fig. 4, for a range of  $T_1$  and  $T_2$  values and flip angles of  $30^\circ$  and  $60^\circ$ . The WC-SSFP contrast is essentially equivalent to the SSFP contrast for a broad range of relaxation parameters considered. Considerable difference is only observed at lower flip angles for  $T_2/T_1 \approx 1$ . Therefore, weighting the SSFP signal by a power of its magnitude prior to combination does not significantly change the basic SSFP contrast provided the power ( $\frac{1}{1+p}$ ) operation is performed.

Phantom images combined with the CS, SOS, nonlinear averaging reconstruction and WC methods are displayed in Fig. 5. The WC-SSFP method achieves better banding artifact suppression than the other combinations as shown by the less noticeable ripples, and has an SNR efficiency comparable to that of the SOS method.

Figure 6 shows in vivo brain images combined with the CS, SOS, and WC methods. The remnants of dark bands

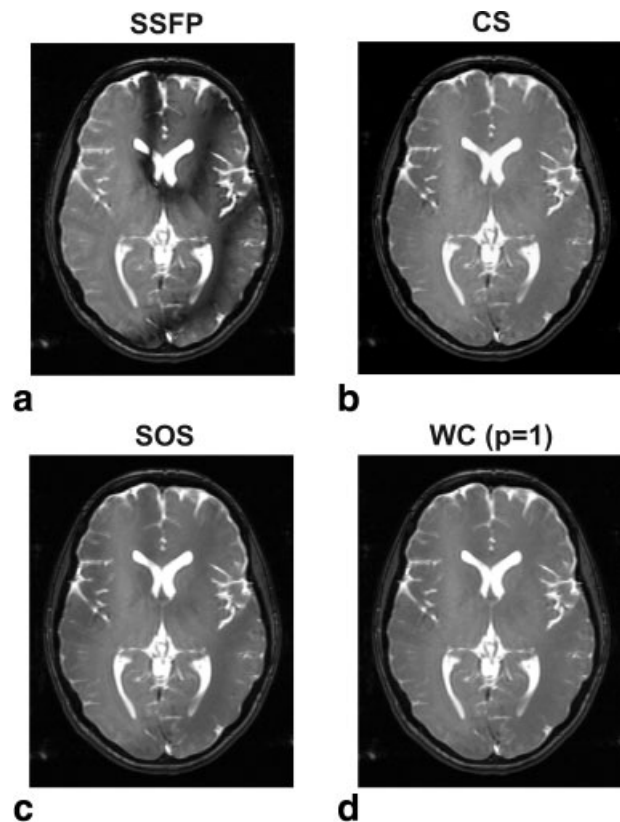


FIG. 6. Two phase-cycled 3DFT-SSFP images of a volunteer's brain were acquired with the following parameters: TR/TE = 15/7.2 ms,  $0.67 \times 1.3 \times 4$  mm<sup>3</sup> resolution,  $\alpha = 30^\circ$ ,  $384 \times 192 \times 16$  encoding, 31.25 kHz readout bandwidth and a total scan time of 1:32. (a) A single SSFP image is displayed (notice the dark bands in the image) along with combination images for (b) CS, (c) SOS, (d) WC ( $p = 1$ ) methods. Identical display windowing was used for all images. The remnants of the dark bands appear in the SOS and CS images, whereas WC-SSFP more successfully reduces the banding artifacts.

in the SSFP acquisitions are still clearly visible in the SOS combination. Although the CS method performs better than the SOS method, the WC-SSFP image has the least noticeable ripples across gray/white matter and CSF. Again, it is important to note that the WC-SSFP combination achieves an SNR close to that of the SOS method.

#### Fat-Water Separation

The phantom images obtained by using the LC-SSFP and WC-SSFP combinations are displayed in Fig. 7. While

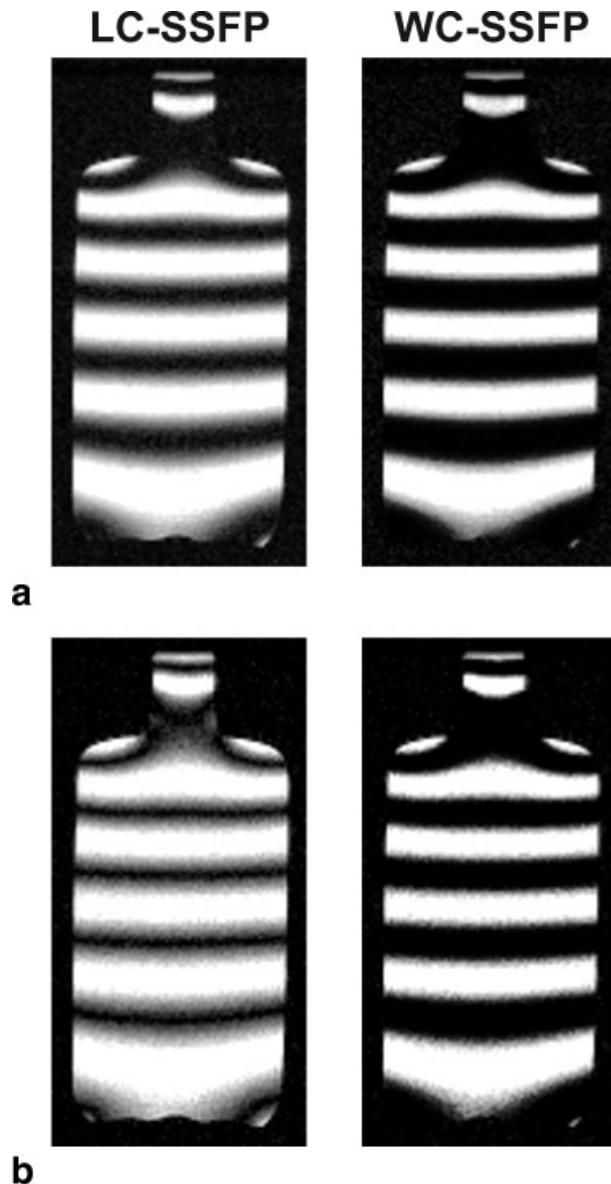


FIG. 7. A 3D SSFP acquisition of a water bottle ( $T_1/T_2 = 250/50$  ms) was accompanied with a linear shim gradient in the readout (vertical) direction to create bands. Identically windowed LC-SSFP and WC-SSFP ( $p = -0.5$ ) images are shown for two different flip angles: (a)  $30^\circ$  and (b)  $60^\circ$ . The remnant stop-band signal depicted as gray regions in the LC-SSFP image appears dark in the WC-SSFP image due to improved suppression. LC-SSFP stop-band suppression gets worse at higher flip angles as predicted; however, WC-SSFP retains its robust stop-band suppression.

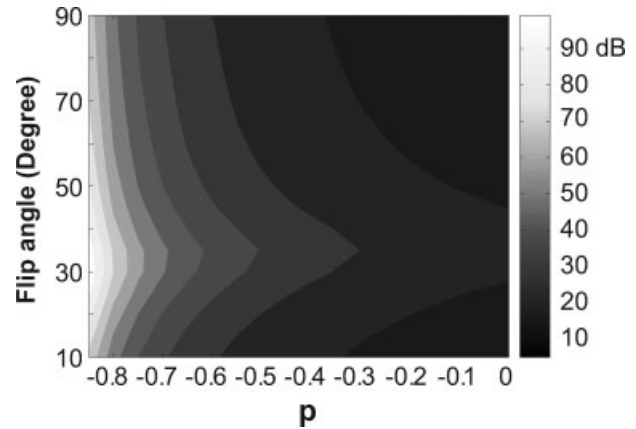


FIG. 8. The contour plot of the logarithm of the ratio of the average pass-band ( $\pm 80$  Hz) signal for water to the average stop-band ( $-220 \pm 80$  Hz) signal for fat as a function of flip angle and the parameter  $p$ .  $TR/TE = 2.3/1.15$  ms,  $T_1/T_2 = 1,000/100$  ms for water and  $T_1/T_2 = 270/85$  ms for fat were assumed for the simulations. The improvement in stop-band suppression as  $p$  is made more negative can be inferred from the increase in the signal ratio.

LC-SSFP images display some residual signal in the stop-bands, the remnant stop-band signal is almost completely suppressed with the WC method ( $p = -0.5$ ). The performance of LC-SSFP degrades at higher flip angles due to the increased inhomogeneity of the SSFP profile. On the other hand, WC-SSFP preserves the robust stop-band signal reduction without compromising the pass-band performance for both flip angles.

The ratio of the average pass-band signal to the average stop-band signal was computed for a range of flip angles and parameter  $p$  as shown in Fig. 8. For a given flip angle, the water-to-fat signal ratio can be computed as a function of the parameter  $p$  and the value of  $p$  that yields the desired signal ratio can be chosen for reconstruction.

The effect of the magnitude-to-a-power weighting on the tissue contrast can be observed by simulating the SSFP signal at the center of the LC-SSFP and WC-SSFP pass-bands for a range of  $T_1$ ,  $T_2$  values and  $30^\circ$  and  $60^\circ$  flip angles. The WC-SSFP method preserves the  $T_2$ -dominant LC-SSFP contrast for which the contributions of  $T_1$  and  $T_2$  can be adjusted through varying the flip angle. Therefore, the magnitude-weighted combination does not alter the targeted tissue contrast.

The coronal and sagittal slices from the in vivo knee images are shown in Fig. 9. There is residual fat signal in the LC-SSFP images, whereas the WC-SSFP method effectively suppresses the fat signal. At  $TR = 2.7$  ms the period of the SSFP spectrum is reduced and the separation between the stop- and pass-bands in LC-SSFP becomes smaller. If the center of the pass-band is aligned with the water resonance, the fat resonance will not exactly be aligned with the center of the stop-band. As a result the stop-band suppression robustness of LC-SSFP is reduced. On the other hand, WC-SSFP achieves robust suppression throughout the stop-band. The greater stop-band suppression with

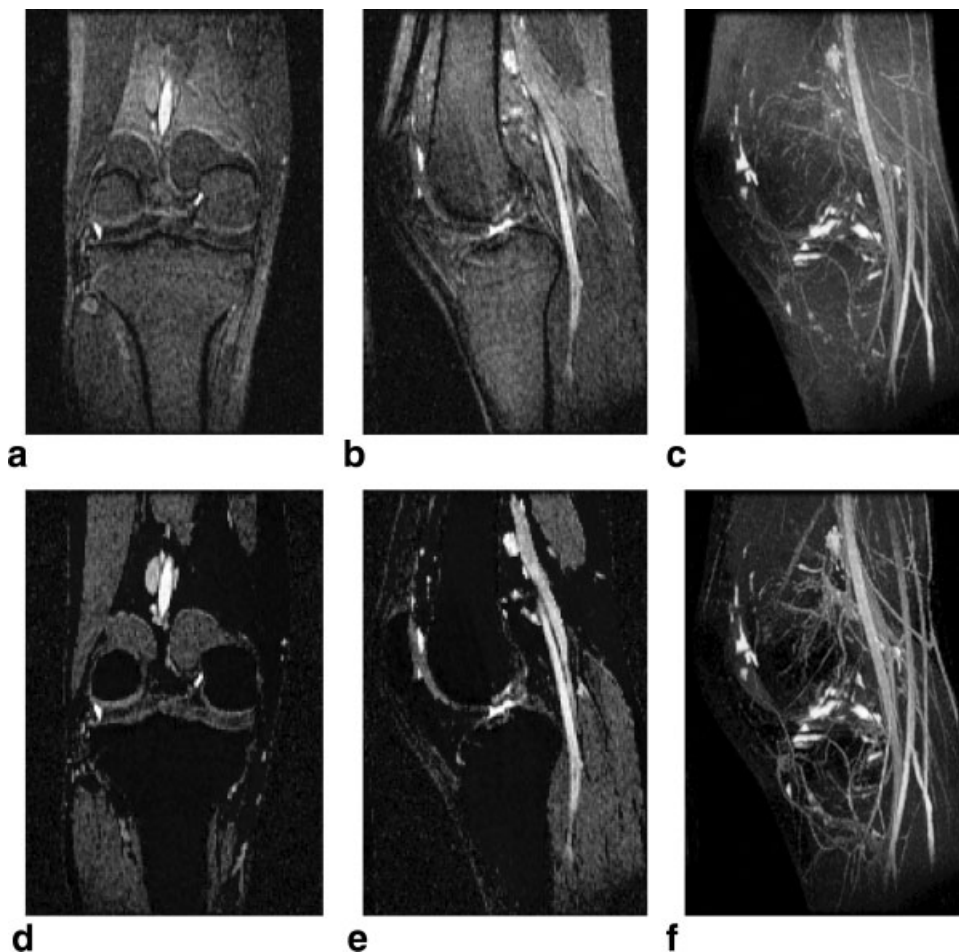


FIG. 9. 3DFT-SSFP images of a volunteer's knee acquired with the following parameters: TR = 2.7 ms, 1 mm isotropic resolution,  $\alpha = 30^\circ$ ,  $192 \times 128 \times 128$  encoding, 250 kHz readout bandwidth and a total scan time of 1:18. Coronal and sagittal slices for (a–b) LC-SSFP and (d–e) WC-SSFP ( $p = -0.5$ ) methods. The corresponding MIPs in the R-L direction are shown in c and f respectively. The vessel depiction in the MIP of the WC-SSFP image is clearly superior because of improved fat suppression.

the WC-SSFP method manifests itself in the maximum-intensity projections (MIPs) with improved depiction of the vasculature.

## DISCUSSION

The signal in fully-refocused SSFP sequences is a function of the resonant frequency. The magnitude spectrum shows signal inhomogeneity and has signal nulls known as banding artifacts. Multiple-acquisition combination methods have been proposed for reducing these artifacts. The sum-of-squares method achieves the highest SNR efficiency; however, it introduces more ripples compared to complex-sum combination. On the other hand, the complex-sum method performs well with banding artifact reduction, but suffers from a loss in SNR due to phase-cancellation effects.

Our WC-SSFP combination is a hybrid method that preserves desirable characteristics of both methods. Even in the optimal SNR case ( $p=1$ ), it can achieve a level of banding-reduction that outperforms the complex-sum and sum-of-squares methods. While achieving robust artifact reduction, it does not sacrifice SNR efficiency as does the complex-sum method. In fact, it achieves an efficiency close to the optimal-SNR SOS combination.  $p=1$  should be used whenever the banding artifact reduction performance of WC-SSFP is acceptable. In applications where better banding artifact reduction is desired, the parameter

$p$  can be used to trade off SNR efficiency for banding artifact reduction. For the considered applications,  $p=4$  seems to significantly improve the performance. Additional flexibility in scan parameter selection, especially TR, will enable SSFP imaging at higher field strengths and with higher resolution.

A common strategy for fat suppression is to create a broad stop-band around the resonant frequency of lipid. There are several methods (e.g., LC-SSFP, FEMR, and FS-ATR) that shape the SSFP profile for this purpose. However, these methods suffer from wedge-shaped stop-bands leading to imperfect fat suppression even when resonant frequency variations are moderate. The WC-SSFP method can dramatically improve stop-band signal suppression compared to LC-SSFP.

Partial-volume effects due to the destructive interference between fat and water spins occupying the same voxel may lead to spurious signal reduction. LC-SSFP does not suffer from partial-volume effects, since the acquisitions are linearly combined. On the other hand, the signals are weighted by a negative power of their magnitude in WC-SSFP, and this non-linearity becomes more pronounced as  $p$  approaches  $-1$ . The magnitude of the signal for a given voxel may be different for the two acquisitions due to the corresponding fat and water phases. This can potentially lead to under- or over-estimation of the signal in the resulting water images due to imperfect cancellation of the

fat signal. Partial-volume effects are actually not noticeable for moderate values of  $|p|$  ( $\leq 0.5$ ). Furthermore, they become less of an issue for high-resolution imaging. At lower resolutions, the value of  $|p|$  should be chosen as small as possible while still effectively suppressing the signal in the stop-band.  $p = -0.5$  significantly improves the stop-band suppression without introducing considerable partial volume artifacts.

Fat-water separation comprising a summation of two SSFP datasets where fat and water are in-phase and out-of-phase has been proposed by Huang et al. (19). However, the method is hindered by imperfect signal cancellation caused by signal heterogeneity because of SSFP nulls. WC-SSFP can be adapted to address this shortcoming. Magnitude-to-a-power weighting of these SSFP signals prior to combination should improve the robustness of fat-water separation and extend the tolerable range of resonant frequency variation. Similarly, WC-SSFP combination can be applied to improve any multiple-acquisition SSFP method that suffers from signal inhomogeneity of the SSFP profile.

## CONCLUSION

The weighted-combination SSFP method is a new multiple-acquisition combination technique that successfully targets two major problems that limit SSFP imaging: banding artifacts and bright fat signal. The robust banding artifact reduction and high SNR efficiency of WC-SSFP combined with the flexibility to fine tune the amount of artifact reduction for a given application extends the applicability of SSFP imaging. Therefore, WC-SSFP can facilitate SSFP imaging at higher fields and in regions of the body where the range of resonant frequency variation is large. It facilitates high-resolution SSFP imaging and SAR reduction by allowing an increase in TR. WC-SSFP can also be used for fat suppression in applications such as coronary artery imaging, cartilage imaging, and flow-independent angiography, where the ability to separate different resonances is valuable. The robust suppression offered combined with the flexibility to adjust the stop-band signal reduction may help to extend the applicability of SSFP imaging.

## REFERENCES

1. Carr HY. Steady-state free precession in nuclear magnetic resonance. *Phys Rev* 1958;112:1693–1701.
2. Oppelt A, Graumann R, Barfuss H, Fischer H, Hartl W, Shajor W. FISP—A new fast MRI sequence. *Electromedica* 1986;54:15–18.
3. Hawkes RC, Patz S. Rapid Fourier imaging using steady-state free precession. *Magn Reson Med* 1987;4:9–23.
4. Scheffler K, Lehnhardt S. Principles and applications of balanced SSFP techniques. *Eur Radiol* 2003;13:2409–2418.
5. Schwenk A. NMR pulse techniques with high sensitivity for slowly relaxing systems. *J Magn Reson* 1971;5:376–389.
6. Zur Y, Wood ML, Neuringer LJ. Motion-insensitive, steady-state free precession imaging. *Magn Reson Med* 1990;16:444–459.
7. Haacke EM, Wielopolski PA, Tkach JA, Modic MT. Steady-state free precession imaging in the presence of motion: Application for improved visualization of the cerebrospinal fluid. *Radiology* 1990;175:545–552.
8. Vasanawala SS, Pauly JM, Nishimura DG. Linear combination steady-state free precession MRI. *Magn Reson Med* 2000;43:82–90.
9. Bangerter NK, Hargreaves BA, Vasanawala SS, Pauly JM, Gold GE, Nishimura DG. Analysis of multiple-acquisition SSFP. *Magn Reson Med* 2004;51:1038–1047.
10. Elliott AM, Bernstein MA, Ward HA, Lane J, Witte RJ. Nonlinear averaging reconstruction method for phase-cycle SSFP. *Magn Reson Imaging* 2007;25:359–364.
11. Deshpande VS, Shea SM, Laub G, Simonetti OP, Finn JP, Li D. 3D magnetization-prepared True-FISP: A new technique for imaging coronary arteries. *Magn Reson Med* 2001;46:494–502.
12. Hargreaves BA, Gold GE, Beaulieu CF, Vasanawala SS, Nishimura DG, Pauly JM. Comparison of new methods for magnetic resonance imaging of articular cartilage. *Magn Reson Med* 2003;49:700–709.
13. Brittain JH, Olcott EW, Szuba A, Gold GE, Wright GA, Irrazaval P, Nishimura DG. Three-dimensional flow-independent peripheral angiography. *Magn Reson Med* 1997;38:343–354.
14. Vasanawala SS, Pauly JM, Nishimura DG. Fluctuating equilibrium MRI. *Magn Reson Med* 1999;42:876–883.
15. Hardy CJ, Dixon WT. Steady-state free precession imaging with inherent fat suppression. In: *Proceedings of the 10th Annual Meeting of ISMRM*. Publisher: ISMRM, Honolulu; 2002. p 473.
16. Overall WR, Nishimura DG, Hu BS. Steady-state sequence synthesis and its application to efficient fat-suppressed imaging. *Magn Reson Med* 2003;50:550–559.
17. Absil J, Denolin V, Metens T. Fat attenuation using a dual steady-state balanced-SSFP sequence with periodically variable flip angles. *Magn Reson Med* 2006;55:343–351.
18. Leupold J, Hennig J, Scheffler K. Alternating repetition time balanced steady state free precession. *Magn Reson Med* 2006;55:557–565.
19. Huang TY, Chung HW, Wang FN, Ko CW, Chen CY. Fat and water separation in balanced steady-state free precession using the Dixon method. *Magn Reson Med* 2004;51:243–247.